Applied Catalysis B: Environmental 136–137 (2013) 19–28

Contents lists available at SciVerse ScienceDirect

Applied Catalysis B: Environmental

journal homepage: www.elsevier.com/locate/apcatb

Novel effect of SO_2 on the SCR reaction over CeO_2: Mechanism and significance

Shijian Yang[a,b,c], Yongfu Guo[d], Huazhen Chang[b], Lei Ma[b], Yue Peng[b], Zan Qu[c], Naiqiang Yan[c], Chizhong Wang[b], Junhua Li[b,*]

[a] School of Environmental and biological Engineering, Nanjing University of Science and Technology, Nanjing, 210094 PR China
[b] State Key Joint Laboratory of Environment Simulation and Pollution Control (SKLESPC), School of Environment, Tsinghua University, Beijing, 100084 PR China
[c] School of Environmental Science and Engineering, Shanghai Jiao Tong University, Shanghai, 200240 PR China
[d] Department of Municipal Engineering, Suzhou University of Science and Technology, Suzhou, 215011, PR China

ARTICLE INFO

Article history:
Received 22 September 2012
Received in revised form 4 December 2012
Accepted 5 January 2013
Available online 7 February 2013

Keywords:
SO_2 effect
CeO_2
Sulfation
NH_3 adsorption
Eley–Rideal mechanism
Catalytic oxidization of NH_3 to NO

ABSTRACT

Ceria (CeO_2) showed a poor activity for the selective catalytic reduction (SCR) of NO with NH_3, while CeO_2 showed an excellent SCR activity in the presence of SO_2 at 300–500 °C. The promotion of SO_2 on the SCR reaction over CeO_2 was mainly due to the sulfation of CeO_2. The SCR reaction over CeO_2 and that over sulfated CeO_2 both followed the Eley–Rideal mechanism (i.e. the reaction between activated NH_3 with gaseous NO). Meanwhile, the catalytic oxidization of NH_3 to NO could simultaneously happen during the SCR reaction, resulting in a drop of NO_x conversion at high temperatures. The adsorption of NH_3 on CeO_2 was obviously promoted after the sulfation, resulting in an obvious promotion of the Eley–Rideal mechanism. Meanwhile, the adsorption sites for —NH_2 adsorption and the oxidization agents for —NH_2 oxidization on CeO_2 were separated after the sulfation. Thus, the probability of the collision between —NH_2 and Ce^{4+} on sulfated CeO_2 was much less than that on CeO_2, resulting in an obvious repression of the catalytic oxidization of NH_3 to NO. As a result, the SCR activity of sulfated CeO_2 was much better than that over CeO_2.

1. Introduction

Nitrogen oxides (NO and NO_2), which result from automobile exhaust gas and industrial combustion of fossil fuels, have been major pollutants for air pollution [1]. Selective catalytic reduction (SCR) with NH_3 is now the most promising technology to control the emission of nitrogen oxides [2]. Although V_2O_5/WO_3-TiO_2 is used as the commercial SCR catalyst for several decades, it is still not satisfactory due to some drawbacks, such as the low N_2 selectivity at high temperatures, the relatively narrow temperature window of 300–400 °C [3], and the toxicity of vanadium pentoxide to the environment [4]. Therefore, a better N_2 selectivity and more environmental-friendly SCR catalyst should be developed.

Recently, it is reported that Ce-based catalysts for example Ce-Cu-Ti oxide [5], CeO_2-WO_3/TiO_2 [6], CeO_2/TiO_2 [7], CeO_2-WO_3 [8] and Ce-W-Ti mixed oxide [9], show excellent SCR activity and N_2 selectivity at 300–400 °C. Ceria (CeO_2) with fluorite structure has attracted tremendous attention for its wide applications in catalysts, fuels, ceramics and gas sensors [10]. Especially, CeO_2 is widely used in three-way catalysis (TWC) to control the emissions of CO, HC, and NO_x from automobile exhaust due to its ability to store oxygen in an oxygen-rich environment while release oxygen in reducing conditions [11]. The SCR activity of CeO_2 was once investigated [12]. CeO_2 showed a poor SCR activity [12]. SCR Catalysts commonly suffer from the severe deactivation induced by SO_2, which is permanently and abundantly present in the exhaust [13]. However, the presence of SO_2 showed an obvious promotion on the SCR reaction over CeO_2, which was quite different from other catalysts. The SCR reaction mechanism over CeO_2 in the presence of SO_2 may differ from that in the absence of SO_2. Actually, the mechanism of SO_2 on the SCR reaction is still not clear. It is important to investigate the mechanism of SO_2 influence on the SCR activity, which is helpful to understand the deactivation/promotion mechanism and further improve its SO_2 durability [14]. Therefore, the mechanism of the SCR reaction over CeO_2 with and without SO_2 was investigated in this work.

2. Experimental

2.1. Preparation

CeO_2 was prepared by the thermal decomposition of $Ce(NO_3)_3{\cdot}6H_2O$ at 550 °C under air for 4 h [12]. Sulfated CeO_2 was obtained by pretreating CeO_2 (1.0 g) in a flow of 400 ppm SO_2 and 2% O_2 (200 mL min^{-1}) at 300 °C for 8 h.

* Corresponding author. Tel.: +86 10 62771093; fax: +86 10 62771093.
E-mail address: lijunhua@tsinghua.edu.cn (J. Li).

0926-3373/$ – see front matter © 2013 Elsevier B.V. All rights reserved.
http://dx.doi.org/10.1016/j.apcatb.2013.01.028

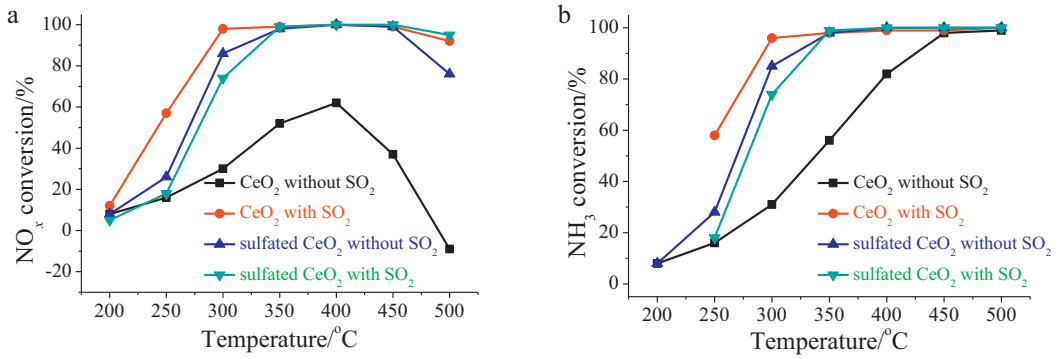

Fig. 1. SCR performance over CeO_2 and sulfated CeO_2: (a), NO_x conversion; (b), NH_3 conversion. Reaction condition: $[NH_3] = [NO] = 500$ ppm, $[O_2] = 2\%$, catalyst mass = 200 mg, total flow rate = 200 mL min^{-1}, GHSV = 60,000 cm^3 g^{-1} h^{-1}.

2.2. Catalytic test

The SCR reaction and the catalytic oxidization of NH_3 and NO were performed on a fixed-bed quartz tube reactor (6 mm of internal diameter). The total flow rate was 200 mL min^{-1} (room temperature), and the mass of catalyst with 40–60 mesh was 200 mg. The corresponding gas hourly space velocity (GHSV) was 6×10^4 cm^3 g^{-1} h^{-1}. The typical reactant gas composition was as follows: 500 ppm of NO (when used), 500 ppm of NH_3 (when used), 400 ppm of SO_2 (when used), 2% of O_2, and balance of N_2. The concentrations of NO, NO_2, NH_3, N_2O and SO_2 were continually monitored by an FTIR spectrometer (MKS Instruments).

2.3. Characterization

BET surface area was determined using a nitrogen adsorption apparatus (Quantachrome, Autosorb-1). Crystal structure was determined using an X-ray diffractionmeter (Rigaku, D/max-2200/PC) between 10° and 80° at a step of 7° min^{-1} operating at 30 kV and 30 mA using Cu Kα radiation. X-ray photoelectron spectroscopy (Thermo, ESCALAB 250) was used to determine the Ce 3d, S 2p, and O 1s binding energies with Al Kα ($h\nu = 1486.6$ eV) as the excitation source. H_2-TPR was recorded on a chemisorption analyzer (Micromeritics, ChemiSorb 2720 TPx) under a 10% hydrogen-90% nitrogen gas flow (50 cm^3 min^{-1}) at a rate of 10 °C min^{-1}. Temperature programmed desorption of ammonia (NH_3-TPD) and temperature programmed desorption of NO (NO-TPD) were carried out on the fixed-bed quartz tube reactor. Before the experiment, about 0.10 g of catalyst was pretreated under N_2 atmosphere at 300 °C for 60 min to remove adsorbed H_2O and other gases. After the catalyst was cooled to 50 °C, the N_2 flow was switched to a flow of 500 ppm NH_3/N_2 or 500 ppm NO + 2% O_2/N_2 (200 mL min^{-1}) for 60 min. The sample was then purged by N_2 (200 mL min^{-1}) for another 60 min. At last, NH_3-TPD (or NO-TPD) was preformed at a heating rate of 10 °C min^{-1} to 600 °C under a N_2 flow (200 mL min^{-1}).

2.4. In situ DRIFTS study

In situ DRIFT spectra were performed on a Fourier transform infrared spectrometer (FTIR, Nicolet NEXUS 870) equipped with a liquid-nitrogen-cooled MCT detector, collecting 100 scans with a resolution of 4 cm^{-1}. The catalyst was first treated with 500 ppm of NO and 2% of O_2, and 500 ppm of NH_3 was then introduced into the IR cell. Subsequently, the reactants were introduced to the catalyst in the reverse order. At last, the IR spectra during the SCR reaction (i.e. 500 ppm of NH_3, 500 ppm of NO and 2% of O_2 were simultaneously introduced) were recorded.

3. Results

3.1. Catalytic performance

3.1.1. Effect of SO_2 on the SCR reaction over CeO_2

Fig. 1a shows the SCR activity of CeO_2 in the absence of SO_2 and that in the presence of SO_2. NO_x conversion over CeO_2 increased from 8% to 62% with the increase of reaction temperature from 200 to 400 °C. Then, NO_x conversion rapidly decreased with the further increase of reaction temperature from 400 to 500 °C. It shows that CeO_2 had a poor SCR activity. During the SCR reaction over CeO_2, only a small amount of N_2O formed (N_2 selectivity was higher than 90%). It is novel that NO_x conversion over CeO_2 obviously increased as 400 ppm of SO_2 was introduced (shown in Fig. 1a). Especially, NO_x conversion over CeO_2 in the presence of SO_2 was close to 100% at 300–450 °C. It indicates that the SCR activity of CeO_2 was obviously promoted due to the presence of SO_2. Furthermore, little N_2O formed during the SCR reaction over CeO_2 in the presence of SO_2, which was much better than that in the absence of SO_2.

3.1.2. Comparison of the SCR reaction over CeO_2 with that over sulfated CeO_2

As is well known, SO_2 can react with metal oxides, resulting in the sulfation of metal oxides [15]. To investigate the mechanism of the promotion of SO_2 on the SCR reaction over CeO_2, the SCR reaction over sulfated CeO_2 was studied. Fig. 1a shows that the SCR activity of CeO_2 was obviously promoted after the sulfation and the presence of SO_2 showed an obvious deactivation of the SCR reaction over sulfated CeO_2. They suggest that the promotion of SO_2 on the SCR reaction over CeO_2 could be mainly due to the sulfation of CeO_2.

Fig. 1b shows NH_3 conversion during the SCR reaction. As shown in Fig. 1b, NH_3 conversion increased in the following sequence: CeO_2 < sulfated CeO_2 < CeO_2 with SO_2, which was consistent with the sequence of NO_x conversion. At 200–350 °C, the ratio of NH_3 conversion over CeO_2 was close to that of NO_x. However, the ratio of NH_3 conversion over CeO_2 was much higher than that of NO_x at 350–500 °C. Especially, NO_x concentration in the outlet was much higher than that in the inlet at 500 °C. They both suggest that some NH_3 was oxidized to NO during the SCR reaction over CeO_2 above 350 °C. As 400 ppm of SO_2 was introduced, the ratio of NH_3 conversion over CeO_2 was close to that of NO_x at 250–450 °C and the ratio of NO_x conversion was slightly less than that of NH_3 at 500 °C. The similar phenomenon also happened to the SCR reaction over sulfated CeO_2.

3.1.3. Effect of the concentration of reactants on the SCR reaction over CeO_2 and sulfated CeO_2

Fig. 2 shows the effect of NO concentration (the ratio of NH_3 to NO was kept at 1:1) on the SCR reaction over CeO_2 and sulfated

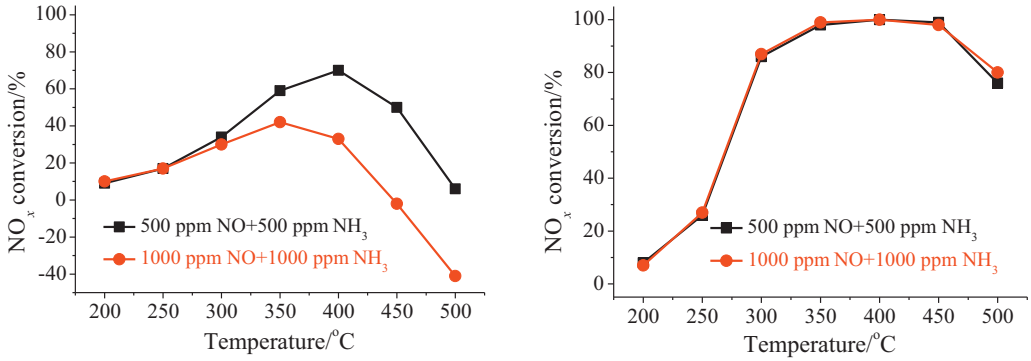

Fig. 2. Effect of the concentrations of NO and NH_3 on the SCR reaction over: (a), CeO_2; (b), sulfated CeO_2. Reaction condition: catalyst mass = 200 mg, total flow rate = 200 mL min^{-1}, GHSV = 60,000 cm^3 g^{-1} h^{-1}.

CeO_2. As the concentrations of NO and NH_3 increased from 500 to 1000 ppm, the ratio of NO_x conversion over CeO_2 did not obviously change at 200–300 °C (shown in Fig. 2a). However, it had an obviously decrease at 350–500 °C. As the concentrations of NO and NH_3 increased from 500 to 1000 ppm, the ratio of NO_x conversion over sulfated CeO_2 at 200–450 °C did not vary (shown in Fig. 2b). However, it slightly increased at 500 °C.

3.2. Characterization

3.2.1. XRD and BET

XRD patterns of CeO_2 and sulfated CeO_2 are shown in Fig. 3. The characteristic peaks of CeO_2 correspond very well to the cubic fluorite structure (JCPDS: 34-0394) [12]. After the sulfation, few changes can be observed in the diffraction scan (shown in Fig. 3). It indicates that the cubic fluorite structure of CeO_2 was not destroyed after the sulfation.

BET surface areas of CeO_2 and sulfated CeO_2 were 53.9 and 24.7 m^2 g^{-1}, respectively. NO_x conversion over sulfated CeO_2 was less than that over CeO_2 in the presence of SO_2 at 200–300 °C (shown in Fig. 1a), which could be related to the lower surface area of sulfated CeO_2.

3.2.2. DRIFT spectra of the sulfation of CeO_2

Fig. 4 shows the DRIFT spectra of the uptake of $SO_2 + O_2$ over CeO_2 at 300 °C. After the introduction of $SO_2 + O_2$ for 30 min, four bands at 1380, 1343, 1107 and 992 cm^{-1} appeared over CeO_2. The band at 1380 cm^{-1} was attributed to asymmetric vibration mode of O═S═O, which was typical "organic" sulfate species with covalent S═O double bands [14]. The bands at 1434, 1107 and 992 cm^{-1} were attributed to chelating bidentate "inorganic" SO_4^{2-}, asymmetric triply degenerate S—O stretching vibration and tetragonal symmetric S—O stretching vibration of free SO_4^{2-}, respectively [16].

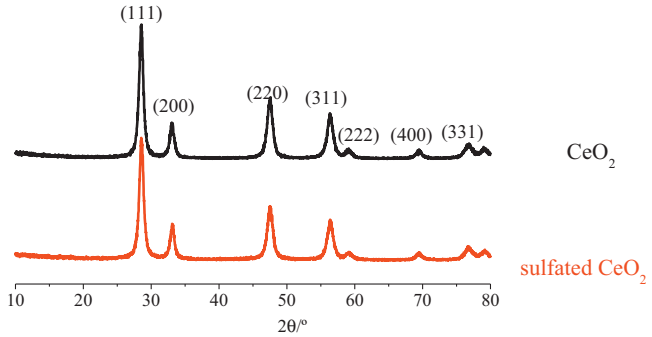

Fig. 3. XRD patterns of CeO_2 and sulfated CeO_2.

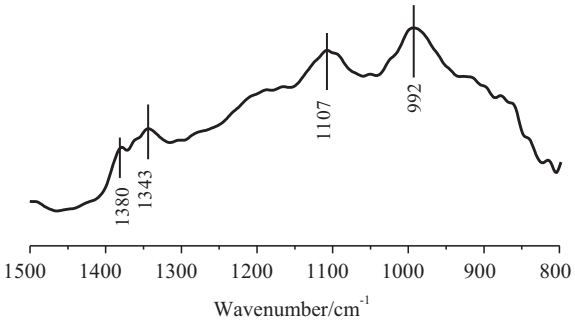

Fig. 4. DRIFT spectra of sulfated CeO_2.

DRIFT spectra demonstrate that CeO_2 had been sulfated after the introduction of $SO_2 + O_2$ to CeO_2 at 300 °C.

3.2.3. XPS

Surface information of CeO_2 and sulfated CeO_2 was analyzed by XPS. XPS spectra over the spectral regions of Ce 3d and S 2p were evaluated (shown in Fig. 5). The Ce 3d binding energies of CeO_2 mainly centered at 901.3, 898.3, 887.2 and 882.1 eV (shown in Fig. 5a), which could be attributed to Ce^{4+} [17]. Meanwhile, the S species on CeO_2 can hardly be observed (shown Fig. 5b).

After the sulfation, two new peaks at 903.2 and 882.8 eV appeared in the spectral region of Ce 3d (shown in Fig. 5c), which could be attributed to $Ce_2(SO_4)_3$. The presence of SO_4^{2-} on sulfated CeO_2 can also be supported by the XPS spectra over S 2p region. The S 2p peaks (shown in Fig. 5d) mainly centered at 168.7 eV and 163.8 eV, which could be assigned to "inorganic" sulfate with ionic S—O bands and "organic" sulfate species with covalent S═O double bands, respectively.

The ratios of Ce, O and S on CeO_2 and sulfated CeO_2 collected from XPS spectra are shown in Table 1. As shown Table 1, the percent of Ce^{4+} on CeO_2 obviously decreased after the sulfation.

3.2.4. TPR

TPR profile recorded from CeO_2 showed three slight reduction peaks (shown in Fig. 6). The reduction peaks at 399, 523 and 766 °C could be assigned to the reduction of surface oxygen species, that of oxygen in deeper interior and that of oxygen in bulk, respectively [18].

Table 1
Ratios of Ce, O and S on CeO_2 and sulfated CeO_2/%.

	Ce^{4+}	Ce^{3+}	O^{2-}	S (SO_4^{2-})
CeO_2	33	0	67	–
Sulfated CeO_2	20	5.0	68	7.0

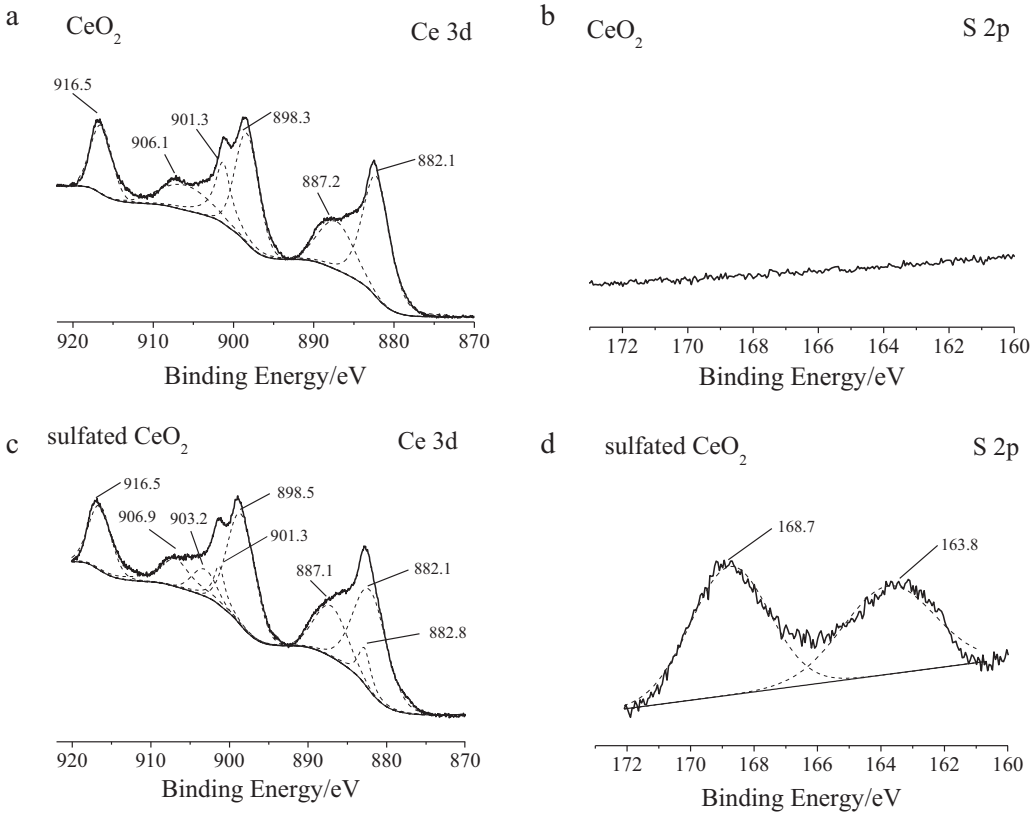

Fig. 5. XPS spectra of CeO_2 and sulfated CeO_2 over the spectral regions of Ce 3d and S 2p.

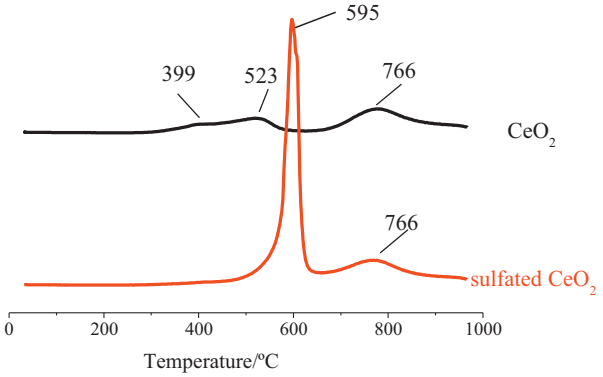

Fig. 6. TPR profiles of CeO_2 and sulfated CeO_2.

After the sulfation, the slight peaks at 399 and 523 °C can not be observed. Meanwhile, a strong peak appeared at 595 °C, which was assigned to the reduction of SO_4^{2-}. TPR analysis also demonstrates that there was some SO_4^{2-} in/on sulfated CeO_2.

3.2.5. Adsorption of NO and NH_3

Table 2 shows the capacities of CeO_2 and sulfated CeO_2 for the adsorption of NO + O_2 and NH_3 at 50 °C, which resulted from NH_3-TPD and NO-TPD analysis (shown in Fig. 7). The capacity of sulfated CeO_2 for NH_3 adsorption was about 7.6 times than that of CeO_2, while the capacity of sulfated CeO_2 for NO + O_2 adsorption was only 14% that of CeO_2. It indicates that the adsorption of NH_3 on CeO_2 was promoted after the sulfation, while the adsorption of NO + O_2 on CeO_2 was restrained.

Table 2
Capacities of CeO_2 and sulfated CeO_2 for NO and NH_3 adsorption at 50 °C/mmol g^{-1}.

	NO	NH_3
CeO_2	1.23	0.5
Sulfated CeO_2	0.17	4.3

Fig. 8 shows the DRIFT spectra of the adsorption of NO + O_2 and NH_3 on CeO_2 and sulfated CeO_2 at 300 °C. The characteristic vibration of NO + O_2 adsorption on CeO_2 mainly appeared at about 1600, 1561, 1528, 1274 and 1216 cm^{-1} (shown in Fig. 8a). The band at 1600 cm^{-1} could be assigned to bridging nitrate, and the bands at 1561, 1528, 1274 and 1216 cm^{-1} could be assigned to bidentate nitrate [19]. After the sulfation, the characteristic vibration of NO + O_2 adsorption on CeO_2 mainly appeared at 1400 cm^{-1}, which was assigned to nitro [19]. The intensity of the adsorption of NO + O_2 on sulfated CeO_2 was much less than that on CeO_2 (shown in Fig. 8a). It indicates that the adsorption of NO + O_2 over CeO_2 was restrained after the sulfation, which was consistent with the result of NO-TPD. Bidentate nitrate and bridging nitrate adsorbed on CeO_2 were coordinated by two of its oxygen atoms, but nitro adsorbed on sulfated CeO_2 was coordinated via its N atom [19]. It suggests that the oxygen atom on CeO_2, which could be used to bridge NO and Ce cation, was covered by SO_4^{2-} after the sulfation. Therefore, the adsorption of NO + O_2 on CeO_2 was restrained after the sulfation, and only nitro formed on sulfated CeO_2.

After the adsorption of NH_3 on CeO_2 at 300 °C, two slight characteristic vibrations at 1547 and 1356 cm^{-1} appeared (shown in Fig. 8b). However, the bands could not be assigned to coordinated ammonia bound to the Lewis acid sites and ionic ammonium bound to the Brønsted acid sites. They could be attributed to monodentate nitrate [19], which resulted from the oxidization of adsorbed NH_3. Two obvious characteristic vibrations appeared at 1431 and 1323 cm^{-1} after the adsorption of NH_3 on sulfated CeO_2 at 300 °C, which were assigned to ammonium ions bound to the Brønsted acid sites [14]. Meanwhile, two negative peaks appeared at 1380 and 1571 cm^{-1}. They could be assigned to sulfate on sulfated CeO_2,

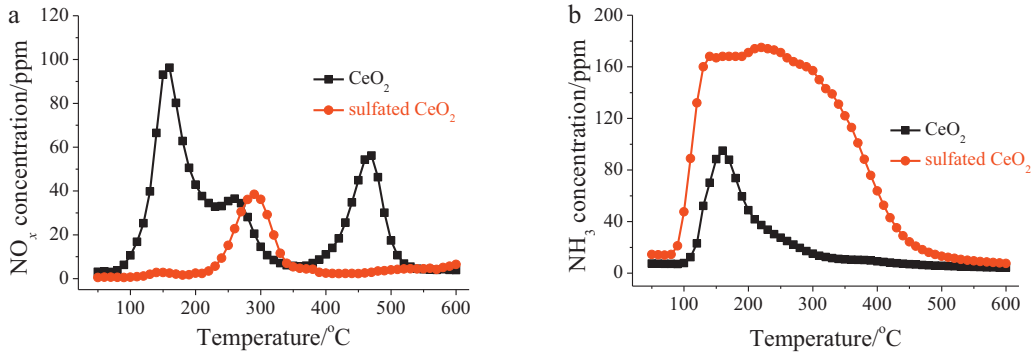

Fig. 7. TPD profiles of CeO_2 and sulfated CeO_2: (a), NO; (b), NH_3.

which was covered by NH_3 [20]. It suggests that NH_3 was mainly adsorbed on SO_4^{2-} on sulfated CeO_2.

3.2.6. Oxidization of NH_3

Fig. 9 shows the results of NH_3 oxidization over CeO_2 and that over sulfated CeO_2. Little NH_3 can be oxidized over CeO_2 blow 300 °C (shown in Fig. 9a). NH_3 oxidization over CeO_2 was promoted with the increase of reaction temperature. However, N_2 selectivity gradually decreased. Above 400 °C, NH_3 was mainly oxidized to NO_x and a small amount of N_2O formed.

NH_3 conversion over sulfated CeO_2 was less than that over CeO_2 (shown in Fig. 9b). It suggests that NH_3 oxidization over CeO_2 was obviously restrained after the sulfation. NH_3 was mainly oxidized to N_2 over sulfated CeO_2, and the formation of NO and NO_2 during NH_3 oxidization over CeO_2 were obviously restrained after the sulfation (shown in Fig. 9b).

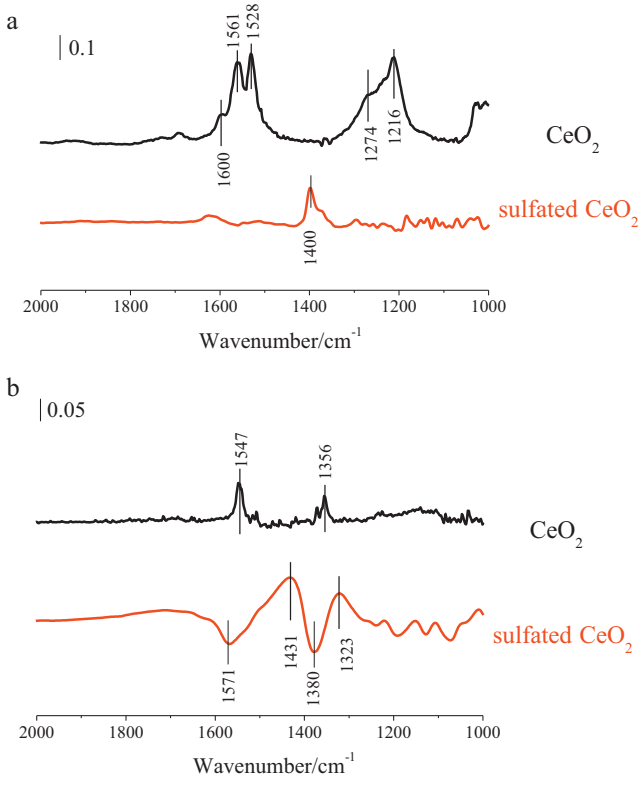

Fig. 8. (a), DRIFT spectra of the adsorption of $NO + O_2$ over CeO_2 and sulfated CeO_2 at 300 °C; (b), DRIFT spectra of the adsorption of NH_3 over CeO_2 and sulfated CeO_2 at 300 °C.

3.2.7. Oxidization of NO

Fig. 10a shows the oxidization of NO over CeO_2 and sulfated CeO_2. The ratio of NO_2 to NO_x over CeO_2 gradually increased to 32% as the reaction temperature increased from 200 to 400 °C. Then, it gradually decreased with the further increase of reaction temperature. With the increase of reaction temperature from 200 to 500 °C, the ratio of NO_2 to NO_x over sulfated CeO_2 gradually increased. Fig. 10a shows that the ratio of NO_2 to NO_x over sulfated CeO_2 was much less than that over CeO_2. It suggests that NO oxidization over CeO_2 was restrained after the sulfation.

Fig. 10b shows NO_2 concentration in the outlet of the SCR reaction over CeO_2 and sulfated CeO_2. The concentration of NO_2 in the outlet obviously increased in the following sequence: the SCR reaction over sulfated CeO_2 with 500 ppm of NO and $NH_3 \approx$ the SCR reaction over sulfated CeO_2 with 1000 ppm of NO and $NH_3 <$ the SCR reaction over CeO_2 with 500 ppm of NO and $NH_3 <$ the SCR reaction over CeO_2 with 1000 ppm of NO and NH_3. However, the SCR activity increased in the reverse sequence (show in Fig. 2). Namely, NO_x conversion decreased with the increase of NO_2 concentration in the outlet. To investigate whether NH_3 was oxidized by NO_2 resulting in the decrease of SCR activity, some NO_2 was introduced into the inlet of the SCR reaction. As 50% of NO in the inlet was substituted by NO_2, NO_x conversion over CeO_2 and that over sulfated CeO_2 both increased (shown in Fig. 11). It suggests that the addition of some NO_2 in the inlet would promote the SCR reaction over CeO_2 and sulfated CeO_2 (i.e. the so-called fast SCR reaction) [21]. Therefore, the lower SCR activity over CeO_2 could not be caused by the higher NO_2 concentration in the outlet.

3.3. In situ DRIFTS study

3.3.1. Reaction between nitrogen oxide and ammonia over CeO_2

CeO_2 was first treated with $NO + O_2/N_2$, and NH_3/N_2 was then introduced into the IR cell (shown in Fig. 12a). After the adsorption of $NO + O_2$ on CeO_2 at 300 °C, CeO_2 was mainly covered by bridging nitrate (at 1600 cm^{-1}) and bidentate nitrate (at 1561, 1528, 1274 and 1216 cm^{-1}). After NH_3/N_2 passed over $NO + O_2/N_2$ pretreated CeO_2 for 10 min, the bands corresponding to bridging nitrate and bidentate nitrate still presented. It suggests that adsorbed NO_x could not take part in the SCR reaction over CeO_2.

Then, the reactants were introduced to CeO_2 in the reverse order. CeO_2 was first treated with NH_3/N_2, and $NO + O_2$ was then introduced into the IR cell (shown in Fig. 12b). After the adsorption of NH_3, CeO_2 was mainly covered by a small amount of monodentate nitrate (at 1547 and 1356 cm^{-1}), which resulted from the oxidization of adsorbed NH_3. After the introduction of $NO + O_2$, CeO_2 was mainly covered by bridging nitrate (at 1600 cm^{-1}) and bidentate nitrate (at 1561, 1530, 1274 and 1216 cm^{-1}).

At last, the IR spectra during the SCR reaction (i.e. NH_3 and $NO + O_2$ were simultaneously introduced) at 300 °C were recorded

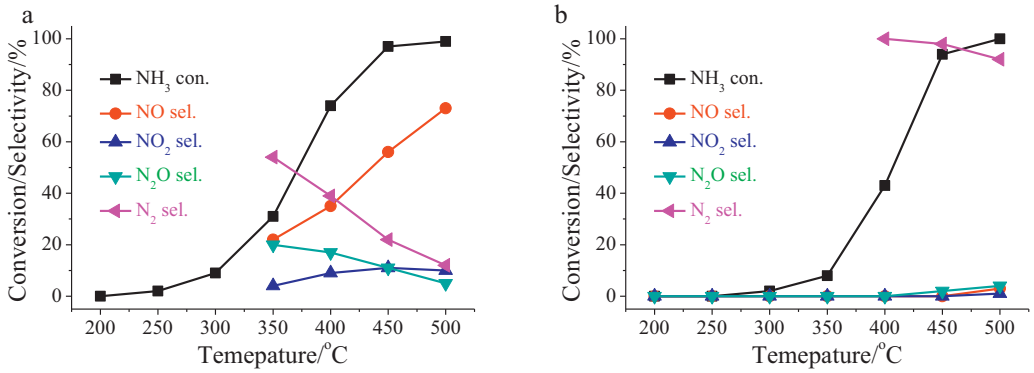

Fig. 9. NH_3 oxidization over: (a), CeO_2; (b), sulfated CeO_2. Reaction condition: $[NH_3]$ = 500 ppm, $[O_2]$ = 2%, catalyst mass = 200 mg, total flow rate = 200 mL min^{-1}, GHSV = 60,000 cm^3 g^{-1} h^{-1}.

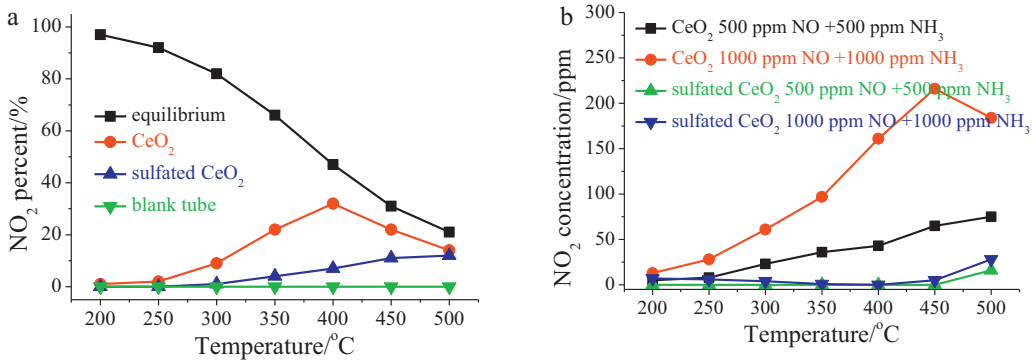

Fig. 10. (a), Oxidization of NO to NO_2 over CeO_2 and sulfated CeO_2, reaction condition: [NO] = 500 ppm, $[O_2]$ = 2%, catalyst mass = 200 mg, total flow rate = 200 mL min^{-1}, GHSV = 60,000 cm^3 g^{-1} h^{-1}; (b), NO_2 concentration in the outlet of the SCR reaction over CeO_2 and sulfated CeO_2, reaction condition: $[O_2]$ = 2%, catalyst mass = 200 mg, total flow rate = 200 mL min^{-1}, GHSV = 60,000 cm^3 g^{-1} h^{-1}.

(shown in Fig. 12c). After the introduction of $NH_3 + NO + O_2$, CeO_2 was mainly covered by bridging nitrate (at 1600 cm^{-1}) and bidentate nitrate (at 1561, 1528, 1274 and 1216 cm^{-1}). Meanwhile, a new band at 1160 cm^{-1} appeared. The band could be attributed to $-NH_2$, which resulted from the activation of coordinated NH_3 bound to the Lewis acid sites [14]. Ce^{4+} on CeO_2 had an excellent oxidization ability [22]. $-NH_2$ adsorbed on CeO_2 can be further oxidized by Ce^{4+} rapidly, so $-NH_2$ can not be observed after the adsorption of NH_3 on CeO_2 (shown in Fig. 8b). Both $-NH_2$ and NO adsorbed on CeO_2 can be oxidized by Ce^{4+} on CeO_2, so NO adsorbed would compete with $-NH_2$ for the oxidization agents (i.e. Ce^{4+} on CeO_2). Table 2 shows that the capacity of CeO_2 for NH_3 adsorption was much less than that of NO. It suggests that the concentration of $-NH_2$ on CeO_2 was much less than that of NO. In balancing the oxidization of NO adsorbed with $-NH_2$ over CeO_2, the former seemed rather to preponderate especially at lower temperatures. Therefore, $-NH_2$ was observed on CeO_2 in the presence of $NO + O_2$ (shown in Fig. 12c). $-NH_2$ can react with gaseous NO to form N_2 and H_2O, so the SCR reaction over CeO_2 could mainly follow the Eley–Rideal mechanism.

3.3.2. *Reaction between nitrogen oxide and ammonia over sulfated CeO_2*

Sulfated CeO_2 was first treated with $NO + O_2/N_2$, and NH_3/N_2 was then introduced into the IR cell (shown in Fig. 13a). After the adsorption of $NO + O_2$ on sulfated CeO_2 at 300 °C, sulfated CeO_2 was mainly covered by nitro (at 1400 cm^{-1}). After NH_3/N_2 passed over $NO + O_2/N_2$ pretreated sulfated CeO_2, the band at 1400 cm^{-1}

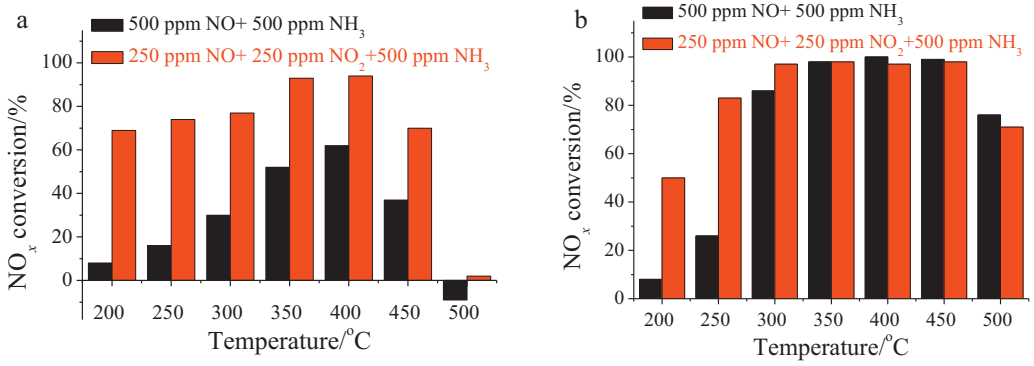

Fig. 11. Effect of NO_2 on the SCR reaction over (a), CeO_2; (b), sulfated CeO_2. Reaction condition: $[O_2]$ = 2%, catalyst mass = 200 mg, total flow rate = 200 mL min^{-1}, GHSV = 60,000 cm^3 g^{-1} h^{-1}.

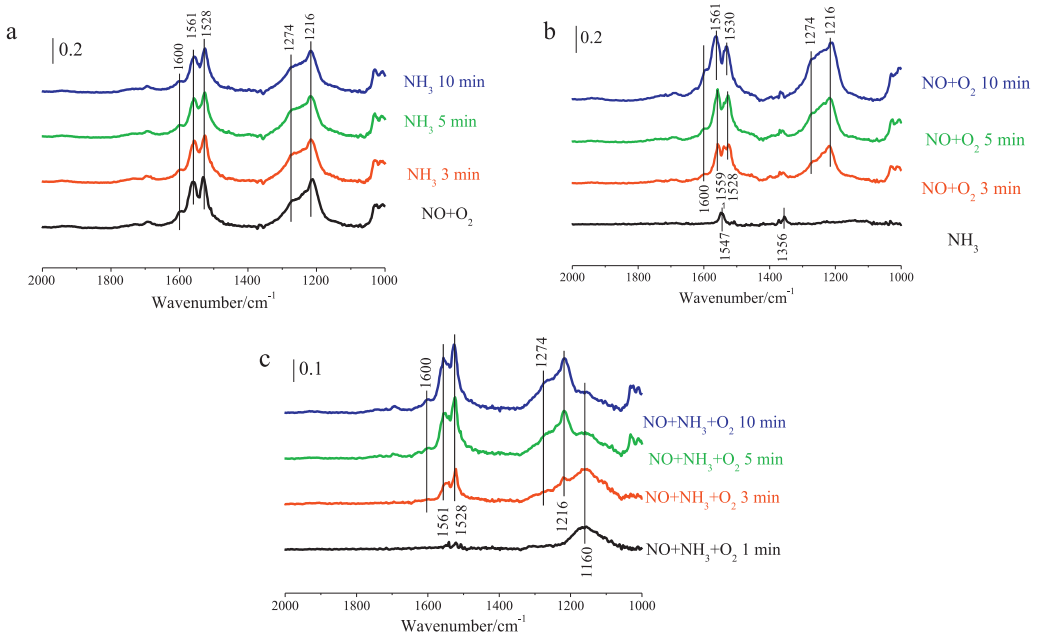

Fig. 12. (a), DRIFT spectra taken at 300 °C upon passing NH_3 over NO + O_2 presorbed CeO_2; (b), DRIFT spectra taken at 300 °C upon passing NO + O_2 over NH_3 presorbed CeO_2; (c), DRIFT spectra taken at 300 °C upon passing NH_3 + NO + O_2 over CeO_2.

corresponding to nitro swiftly diminished, and sulfated CeO_2 was mainly covered by ionic NH_4^+ bound to the Brønsted acid sites (at 1431 and 1323 cm^{-1}). It indicates that the reaction between adsorbed NO_x (nitro) and NH_3 could contribute to the SCR reaction over sulfated CeO_2.

Then, the reactants were introduced to sulfated CeO_2 in the reverse order (shown in Fig. 13b). After the adsorption of NH_3 at 300 °C, sulfated CeO_2 was mainly covered by ionic NH_4^+ bound to SO_4^{2-} (1431 and 1323 cm^{-1}). After NO + O_2/N_2 passed over NH_3/N_2 pretreated sulfated CeO_2, ionic NH_4^+ diminished, and sulfated CeO_2 was mainly covered by nitro (at 1400 cm^{-1}). Meanwhile, a new band at 1628 cm^{-1} appeared, which could be assigned to adsorbed H_2O resulted from the SCR reaction [23]. They both demonstrate that the reaction between adsorbed NH_3 and NO would contribute to the SCR reaction over sulfated CeO_2.

At last, the IR spectra during the SCR reaction over sulfated CeO_2 at 300 °C were recorded. As shown in Fig. 13c, the bands at 1431 and 1323 cm^{-1} corresponding to ionic NH_4^+ bound to SO_4^{2-} appeared. However, the band at 1400 cm^{-1} corresponding to nitro was not observed. NH_3 mainly adsorbed on SO_4^{2-} on sulfated CeO_2, while

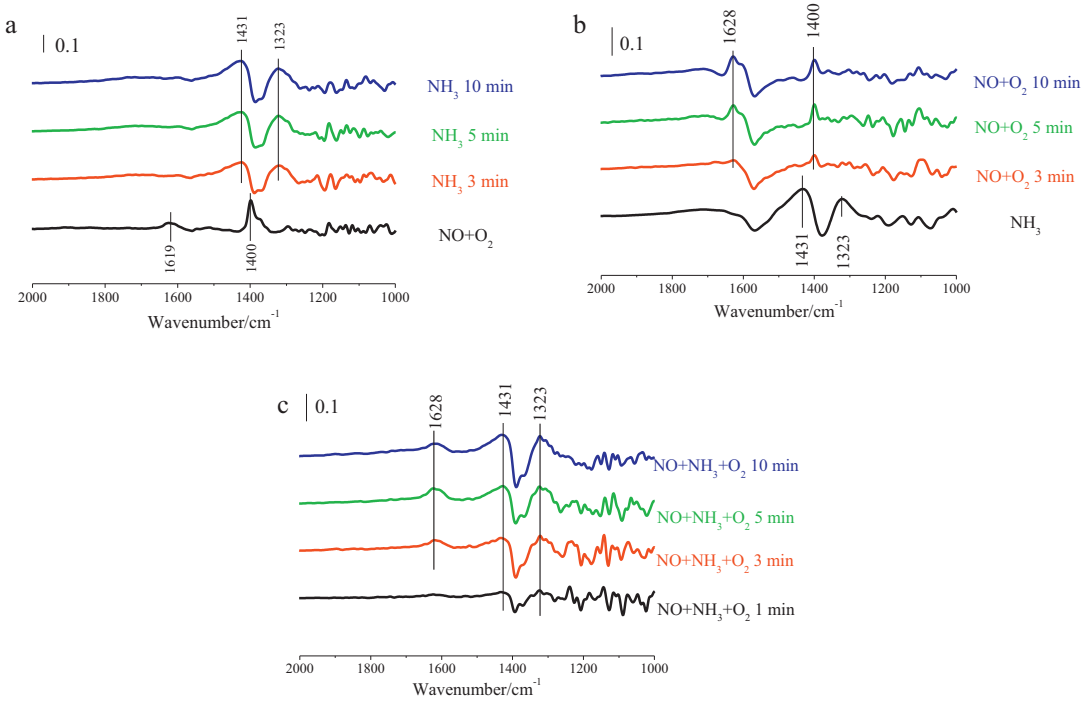

Fig. 13. (a), DRIFT spectra taken at 300 °C upon passing NH_3 over NO + O_2 presorbed sulfated CeO_2; (b), DRIFT spectra taken at 300 °C upon passing NO + O_2 over NH_3 presorbed sulfated CeO_2; (c), DRIFT spectra taken at 300 °C upon passing NH_3 + NO + O_2 over sulfated CeO_2.

NO mainly adsorbed on Ce^{4+} (or Ce—O band) on sulfated CeO_2. Therefore, NH_3 did not compete with NO for the adsorption sites on sulfated CeO_2. However, NH_3 and NO adsorbed can be oxidized by Ce^{4+} on sulfated CeO_2 to $-NH_2$ and nitro respectively, so NH_3 adsorbed would compete with NO adsorbed for the oxidization agents (i.e. Ce^{4+} on sulfated CeO_2). Table 2 shows that the capacity of sulfated CeO_2 for NH_3 adsorption was about 25 times that of NO. Therefore, Ce^{4+} on sulfated CeO_2 preferred to activate adsorbed NH_3 rather than to oxidize adsorbed NO. As a result, nitro could not form over sulfated CeO_2 during the SCR reaction. It suggests that the SCR reaction over sulfated CeO_2 mainly followed the Eley–Rideal mechanism.

4. Discussion

In situ DRIFTS study suggests that the SCR reaction over CeO_2 and sulfated CeO_2 mainly followed the Eley–Rideal mechanism (i.e. reaction of activated ammonia with gaseous NO). The SCR reaction over CeO_2 and sulfated CeO_2 through the Eley–Rideal mechanism can be approximately described as follows [24]:

$$NH_{3(g)} \leftrightharpoons NH_{3(ad)} \quad (1)$$

$$NH_{3(ad)} + \equiv Ce^{4+} \rightarrow -NH_2 + \equiv Ce^{3+} + H^+ \quad (2)$$

$$-NH_2 + NO_{(g)} \rightarrow N_2 + H_2O \quad (3)$$

$$\equiv Ce^{3+} + 1/4O_2 \rightarrow \equiv Ce^{4+} + 1/2 \equiv O^{2-} \quad (4)$$

Reaction (1) was the adsorption of gaseous ammonia on the acid sites. Reaction (2) was the activation of adsorbed NH_3 by Ce^{4+} on the surface to form $-NH_2$. $-NH_2$ then reacted with gaseous NO to form N_2 and H_2O (Reaction (3)). Reaction (4) was the regeneration of Ce^{4+}.

NH_3 oxidization could simultaneously happen during the SCR reaction over CeO_2 and sulfated CeO_2 above 300 °C (shown in Fig. 9), and it can be described as [25]:

$$NH_{3(g)} \leftrightharpoons NH_{3(ad)} \quad (1)$$

$$NH_{3(ad)} + \equiv Ce^{4+} \rightarrow -NH_2 + \equiv Ce^{3+} + H^+ \quad (2)$$

$$-NH_2 + O_2 \xrightarrow{\equiv Ce^{4+}} NO + H_2O \quad (5)$$

$$-NH_2 + NO_{(g)} \rightarrow N_2 + H_2O \quad (3)$$

$$\equiv Ce^{3+} + 1/4O_2 \rightarrow \equiv Ce^{4+} + 1/2 \equiv O^{2-} \quad (4)$$

$-NH_2$ can be further catalytically oxidized to NO by Ce^{4+} on the surface at high temperatures (Reaction (5)). Then, the formed NO from NH_3 oxidization can also be reduced by $-NH_2$ to N_2 through Reaction (3). It was the so-called selective catalytic oxidization of NH_3 [26].

The kinetic equation of the activation of adsorbed NH_3 (Reaction (2)) can be described as [20]:

$$-\frac{d[NH_{3(ad)}]}{dt} = -\frac{d\left[\equiv Ce^{4+}\right]}{dt} = \frac{d[-NH_2]}{dt} = k_1\left[NH_{3(ad)}\right]\left[\equiv Ce^{4+}\right] \quad (6)$$

where, k_1, $[NH_{3(ad)}]$, $[\equiv Ce^{4+}]$ and $[-NH_2]$ were the kinetic constant of Reaction (2), the concentrations of adsorbed NH_3, Ce^{4+} and $-NH_2$ on the surface, respectively.

The kinetic equation of the reduction of gaseous NO by activated NH_3 (Reaction (3)) can be described as [27]:

$$-\frac{d[-NH_2]}{dt} = -\frac{d[NO_{(g)}]}{dt} = k_2[-NH_2][NO_{(g)}] \quad (7)$$

where, k_2 and $[NO_{(g)}]$ were the kinetic constant of Reaction (3) and the concentration of gaseous NO, respectively.

The kinetic equation of the catalytic oxidization of activated NH_3 to NO (Reaction (5)) can be approximately described as:

$$-\frac{d[-NH_2]}{dt} = -\frac{d\left[\equiv Ce^{4+}\right]}{dt} = k_3[-NH_2]\left[\equiv Ce^{4+}\right] \quad (8)$$

where, k_3 was the kinetic constant of Reaction (5).

According to Eqs. (7) and (8), the consumption of NH_2 (i.e. NH_3 conversion) can be approximately described as:

$$-\frac{d[-NH_2]}{dt} = k_3[-NH_2]\left[\equiv Ce^{4+}\right] + k_2[-NH_2]\left[NO_{(g)}\right] \quad (9)$$

The contributions of the catalytic oxidization of NH_3 to NO (i.e. Reaction (5)) and the SCR reaction through the Eley–Rideal mechanism (i.e. Reaction (3)) to NH_3 conversion (i.e. $-NH_2$ oxidization) can be calculated according to the difference between NH_3 conversion and NO_x conversion. Fig. 14 shows the contributions of the Eley–Rideal mechanism and the catalytic oxidization of NH_3 to NO to NH_3 conversion during NH_3 oxidization and the SCR reaction over CeO_2 and sulfated CeO_2. The catalytic oxidization of NH_3 to NO predominated over NH_3 oxidization over CeO_2 and only a small amount NH_3 conversion was related to the SCR reaction through the Eley–Rideal mechanism (shown in Fig. 14a). Eq. (7) shows that the SCR reaction through the Eley–Rideal mechanism would be promoted with the increase of gaseous NO concentration. Therefore, NH_3 conversion over CeO_2 through the SCR reaction with the Eley–Rideal mechanism was remarkably promoted as 500 ppm of NO was introduced, resulting in the increase of NH_3 conversion (shown in Fig 14a and c). Reaction (3) would compete with Reaction (5) for the consumption of $-NH_2$ (shown in the Eq. (9)). As NH_3 conversion through the Eley–Rideal mechanism (Reaction (3)) was promoted after the introduction of 500 ppm of NO, NH_3 conversion through the catalytic oxidization of NH_3 to NO (Reaction (5)) was obviously restrained (shown in Fig. 14a and c). The similar result was also observed on sulfated CeO_2 (show in Fig. 14b and d).

NH_3 conversion through the catalytic oxidization of NH_3 to NO during the SCR reaction over CeO_2 was completely suppressed at 350–400 °C after the sulfation, and only a small amount of NH_3 conversion over sulfated CeO_2 above 450 °C was related to Reaction (5). Meanwhile, NH_3 conversion during the SCR reaction over CeO_2 through the Eley–Rideal mechanism was obviously promoted after the sulfation, resulting in the remarkable promotion of NH_3 conversion at 250–400 °C (shown in Fig. 14c and d).

The acid sites on CeO_2 (Lewis acid) mainly resulted from the unsaturated coordination between Ce^{4+} and O^{2-}, while the acid sites on sulfated CeO_2 (Brønsted acid) mainly resulted from SO_4^{2-} on the surface. Therefore, NH_3 mainly adsorbed on Ce^{4+} (or Ce—O band) on CeO_2, while it mainly adsorbed on SO_4^{2-} on sulfated CeO_2. Thus, the probability of the collision between NH_3 adsorbed and Ce^{4+} on sulfated CeO_2 was much less than that on CeO_2. It suggests that k_1 of sulfated CeO_2 was much less than that of CeO_2. Meanwhile, the concentration of Ce^{4+} on sulfated CeO_2 was less than that on CeO_2 (shown in Table 1). They both caused the deactivation of CeO_2 for the SCR reaction, which was consistent with CeO_2/TiO_2 [28]. However, the capacity of CeO_2 for NH_3 adsorption increased about 8 times after the sulfation (shown in Table 2). As a result, the activation of adsorbed NH_3 on CeO_2 was promoted after the sulfation due to the remarkable increase of the concentration of NH_3 adsorbed (hinted by Eq. (6)). It suggests that the concentration of $-NH_2$ on sulfated CeO_2 was more than that on CeO_2. Therefore, the SCR reaction over CeO_2 through the Eley–Rideal mechanism was promoted after the sulfation (hinted by Eq. (7)), which was demonstrated by Fig. 14c and d.

With the increase of reaction temperature, the catalytic oxidization of $-NH_2$ to NO (Reaction (5)) happened. $-NH_2$ mainly adsorbed on Ce^{4+} (or Ce—O band) on CeO_2, while it mainly adsorbed on SO_4^{2-} on sulfated CeO_2. Therefore, the probability of the collision between

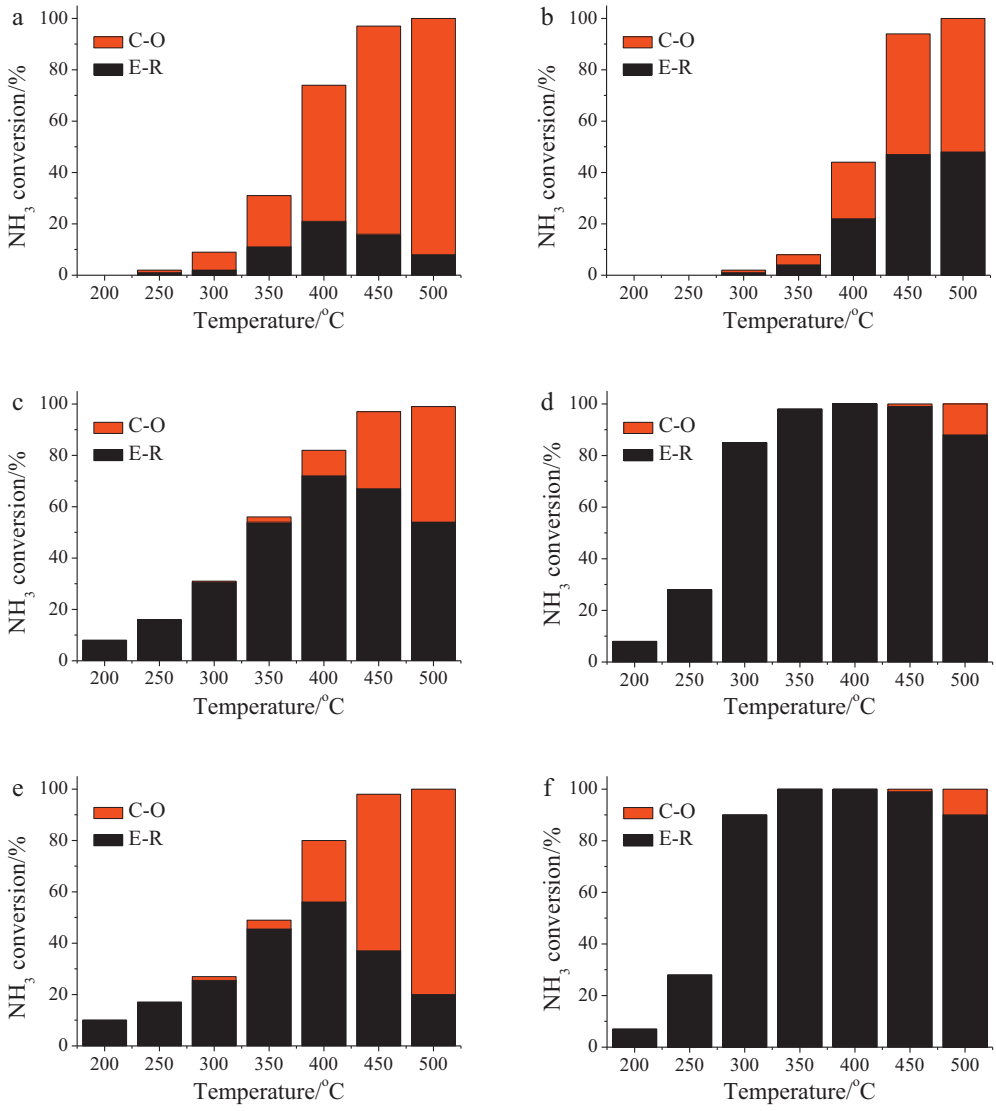

Fig. 14. Contributions of the Eley–Rideal mechanism (E–R) and the catalytic oxidization of NH_3 to NO (C—O) to NH_3 conversion over: (a), CeO_2, [NH_3] = 500 ppm; (b), sulfated CeO_2, [NH_3] = 500 ppm; (c), CeO_2, [NH_3] = [NO] = 500 ppm; (d), sulfated CeO_2, [NH_3] = [NO] = 500 ppm; (e), CeO_2, [NH_3] = [NO] = 1000 ppm; (f), sulfated CeO_2, [NH_3] = [NO] = 1000 ppm. Reaction condition: [O_2] = 2%, catalyst mass = 200 mg, total flow rate = 200 mL min^{-1}, GHSV = 60,000 cm^3 g^{-1} h^{-1}.

—NH_2 and Ce^{4+} on sulfated CeO_2 was much less than that on CeO_2. It suggests that k_3 of sulfated CeO_2 was much less than that of CeO_2. Meanwhile, the concentration of Ce^{4+} on sulfated CeO_2 was less than that on CeO_2. Although the concentration of —NH_2 on sulfated CeO_2 was more than that on CeO_2, the increase of —NH_2 concentration on CeO_2 after the sulfation was much less than that of NH_3. As a result, the catalytic oxidization of —NH_2 to NO was obviously suppressed after the sulfation (hinted by Eq. (8)), which was demonstrated by Fig. 14c and d. After the sulfation, the SCR reaction over CeO_2 through the Eley–Rideal mechanism was promoted, and the catalytic oxidization of —NH_2 to NO over CeO_2 was obviously restrained. Therefore, NO_x conversion over sulfated CeO_2 was much higher than that over CeO_2.

Both NH_3 and NO mainly adsorbed on Ce^{4+} on CeO_2, so NH_3 would compete with NO + O_2 for the adsorption sites on CeO_2. The increase of NH_3 concentration in gas phase would promote the adsorption of NH_3 in the presence of NO. Therefore, the concentration of NH_3 adsorbed (i.e. the concentration of —NH_2) on CeO_2 would obviously increase and the concentration of NO adsorbed on CeO_2 would decrease as the concentration of NH_3 increased from 500 to 1000 ppm. Because of the decrease of NO adsorbed and the increase of —NH_2 on CeO_2, Ce^{4+} on CeO_2 preferred to oxidize —NH_2 rather than to oxidize NO adsorbed. Therefore, the catalytic oxidization of —NH_2 to NO was promoted with the increase of NH_3 and NO concentrations from 500 to 1000 ppm (shown in Fig. 14c and e), resulting in an obvious decrease of NO_x conversion above 300 °C (shown in Fig. 2a).

The SCR reaction over sulfated CeO_2 mainly followed the Eley–Rideal mechanism (shown in Fig. 14d and f). If the SCR reaction mainly followed the Eley–Rideal mechanism, the reaction orders with respect to the concentrations of gaseous NH_3 and NO were 0 and 1, respectively [20]. Therefore, the ratio of NO_x conversion over sulfated CeO_2 did not change with the increase of NO and NH_3 concentrations from 500 to 1000 ppm at 200–450 °C (shown in Fig. 2b). At 500 °C, some NH_3 conversion over sulfated CeO_2 was related to the catalytic oxidization of NH_3 to NO. Reaction 3 would compete with Reaction 5 for the consumption of —NH_2 (shown in Eq. (9)). As the concentration of gaseous NO increased, Reaction (3) was promoted (hinted by Eq. (7)). It suggests that the catalytic oxidization of NH_3 to NO over sulfated CeO_2 was restrained due to the increase of NO concentration (shown in Fig. 14d and f). As a result, NO_x conversion over sulfated CeO_2 at 500 °C slightly increased as NH_3

and NO concentrations increased from 500 to 1000 ppm (shown in Fig. 2b).

A small amount of SO_2 was observed in the outlet during the SCR reaction over sulfated CeO_2 at 500 °C. It indicates that some SO_4^{2-} on sulfated CeO_2 was decomposed at 500 °C. The decomposition of SO_4^{2-} on sulfated CeO_2 could be restrained in the presence of SO_2. Therefore, NO_x conversion over sulfated CeO_2 was less than that over CeO_2 and sulfated CeO_2 in the presence of SO_2 at 500 °C (shown in Fig. 1a).

5. Conclusion

The promotion of SO_2 on the SCR reaction over CeO_2 was mainly related to the sulfation of CeO_2. The SCR reaction over CeO_2 and that over sulfated CeO_2 mainly followed the Eley–Rideal mechanism, and the catalytic oxidization of NH_3 to NO simultaneously happened at high temperatures. The capacity of CeO_2 for NH_3 adsorption was very low, so the SCR reaction over CeO_2 through the Eley–Rideal mechanism was very weak. Furthermore, $-NH_2$ was mainly adsorbed on Ce^{4+} on CeO_2, which would be easily oxidized by Ce^{4+} to NO at high temperatures. Therefore, NO_x conversion over CeO_2 gradually decreased above 400 °C. As a result, CeO_2 showed a poor SCR activity. The adsorption of NH_3 over CeO_2 was obviously promoted after the sulfation, resulting in an obvious promotion of the Eley–Rideal mechanism. The sites for $-NH_2$ adsorption and the oxidization agents for $-NH_2$ oxidization on CeO_2 were separated after the sulfation, resulting in an obvious inhibition of the catalytic oxidization of $-NH_2$ to NO. As a result, the SCR activity of CeO_2 obviously increased after the sulfation.

Acknowledgments

This study was financially supported by the National Natural Science Fund of China (Grant Nos. 21207067 and 51078203), special fund of State Key Joint Laboratory of Environment Simulation and Pollution Control, and the National High-Tech Research and Development (863) Program of China (Grant Nos. 2010AA065002 and 2012AA062506).

References

[1] G.S. Qi, R.T. Yang, Journal of Catalysis 217 (2003) 434–441.
[2] N.Y. Topsoe, Science 265 (1994) 1217–1219.
[3] G.S. Qi, R.T. Yang, Applied Catalysis B: Environmental 44 (2003) 217–225.
[4] L. Chen, J.H. Li, M.F. Ge, Enviornmental Science and Technology 44 (2010) 9590–9596.
[5] X. Gao, X.S. Du, L.W. Cui, Y.C. Fu, Z.Y. Luo, K.F. Cen, Catalysis Communications 12 (2010) 255–258.
[6] L. Chen, J.H. Li, M.F. Ge, R.H. Zhu, Catalysis Today 153 77-83.
[7] W.P. Shan, F.D. Liu, H. He, X.Y. Shi, C.B. Zhang, Catalysis Today 184 (2012) 160–165.
[8] W.P. Shan, F.D. Liu, H. He, X.Y. Shi, C.B. Zhang, Chemical Communications 47 (2011) 8046–8048.
[9] W.P. Shan, F.D. Liu, H. He, X.Y. Shi, C.B. Zhang, Applied Catalysis B: Environmental 115 (2012) 100–106.
[10] W. Cen, Y. Liu, Z. Wu, H. Wang, X. Weng, Physical Chemistry Chemical Physics 14 (2012) 5769–5777.
[11] M. Epifani, T. Andreu, S. Abdollahzadeh-Ghom, J. Arbiol, J.R. Morante, Advanced Functional Materials 22 (2012) 2867–2875.
[12] T.T. Gu, Y. Liu, X.L. Weng, H.Q. Wang, Z.B. Wu, Catalysis Communications 12 (2010) 310–313.
[13] G.Y. Xie, Z.Y. Liu, Z.P. Zhu, Q.Y. Liu, J. Ge, Z.G. Huang, Journal of Catalysis 224 (2004) 36–41.
[14] F.D. Liu, K. Asakura, H. He, W.P. Shan, X.Y. Shi, C.B. Zhang, Applied Catalysis B: Environmental 103 (2011) 369–377.
[15] H.B. Fu, X. Wang, H.B. Wu, Y. Yin, J.M. Chen, Journal of Physical Chemistry C 111 (2007) 6077–6085.
[16] M. Waqif, P. Bazin, O. Saur, J.C. Lavalley, G. Blanchard, O. Touret, Applied Catalysis B: Environmental 11 (1997) 193–205.
[17] L. Chen, J.H. Li, M.F. Ge, Journal of Physical Chemistry C 113 (2009) 21177–21184.
[18] M. Sun, G. Zou, S. Xu, X. Wang, Materials Chemistry and Physics 134 (2012) 912–920.
[19] K.I. Hadjiivanov, Catalysis Reviews 42 (2000) 71–144.
[20] S.J. Yang, J.H. Li, C.Z. Wang, J.H. Chen, L. Ma, H.Z. Chang, L. Chen, Y. Peng, N.Q. Yan, Applied Catalysis B: Environmental 117 (2012) 73–80.
[21] E. Tronconi, I. Nova, C. Ciardelli, D. Chatterjee, M. Weibel, Journal of Catalysis 245 (2007) 1–10.
[22] M.J. Sun, G.J. Zou, S. Xu, X.L. Wang, Materials Chemistry and Physics 134 (2012) 912–920.
[23] S.J. Yang, C.Z. Wang, J.H. Chen, Y. Peng, L. Ma, H.Z. Chang, L. Chen, C.X. Liu, J.Y. Xu, J.H. Li, N.Q. Yan, Catalysis Science & Technology 2 (2012) 915–917.
[24] G. Busca, L. Lietti, G. Ramis, F. Berti, Applied Catalysis B: Environmental 18 (1998) 1–36.
[25] G.Y. Xie, Z.Y. Liu, Z.P. Zhu, Q.Y. Liu, J. Ge, Z.G. Huang, Journal of Catalysis 224 (2004) 42–49.
[26] R.Q. Long, R.T. Yang, Journal of Catalysis 207 (2002) 158–165.
[27] S. Yang, C. Wang, J. Li, N. Yan, L. Ma, H. Chang, Applied Catalysis B: Environmental 110 (2011) 71–80.
[28] W.Q. Xu, H. He, Y.B. Yu, Journal of Physical Chemistry C 113 (2009) 4426–4432.